Theory of the electric-field gradient in dilute alloys

S. Prakash and S. K. Rattan
Department of Physics, Panjab University, Chandigarh-160014, India

J. Singh
Department of Physics, Punjab Agricultural University, Ludhiana-141004, India
(Received 23 December 1992; revised manuscript received 28 April 1993)

A unified theory of the electric-field gradient (EFG) in binary metallic alloys is proposed. The valence and size EFGs are generated simultaneously from crystal potentials for the perfect and imperfect lattices. Dielectric-screening theory is used to calculate the two-body potential and the crystal potential for dilute alloys. The anisotropy of the strain field is studied and it is found that the strain field becomes negligibly small beyond twenty-five nearest neighbors of the impurity. The EFGs are calculated at the displaced first- and second-nearest-neighbor positions without introducing any size strength parameter for *Al*(Mg, Zn, Sn) and *Cu*(Mg, Zn, Sn) alloys. The calculated values are found in good agreement with the experimental values. The valence EFG is dominant at the first-nearest neighbor while size EFG starts dominating at farther nearest neighbors.

I. INTRODUCTION

A point defect in a metal reduces the symmetry of the lattice that can be ascribed to two physical processes.[1,2] First the valence difference between the host and impurity atoms creates scattering centers that scatter the conduction electrons of the host metal, producing a charge perturbation around the point defect. This gives rise to a point-defect-induced excess potential. It is called the valence effect and the electric-field gradient (EFG) so produced is valence EFG. Second, the different size of the defect atom alters the force constants causing strain in the lattice. It makes host atoms move to new equilibrium positions. In the strained lattice the conduction electrons are further redistributed producing an additional change in the crystal potential. It is called size effect and the EFG so produced is size EFG. The above two perturbations polarize the ion cores of the host and hence produce antishielding effects which substantially modify the EFG at the nuclear site. It is taken care of by introducing the Sternheimer antishielding factor.

The valence and size effects are interrelated. Therefore the calculations of defect-induced potentials and EFGs become involved. However, the artificial separation of the valence and size effects has made the problem tractable.[3–8] In general, in the evaluation of EFG one calculates change in the electron density and hence the change in the electrostatic potential. In the valence EFG these quantities are calculated using free-electron theory,[3] nearly free-electron theory,[5] and jellium model of metals.[6,7] Sagalyn and co-workers[4,9] emphasized the importance of the strain field and evaluated the size EFG in the continuum model of the lattice by introducing size strength parameter. The same model is used later by a number of workers.[2] Hafizuddin and Mohapatra[8] evaluated the size EFG for a vacancy using a semidiscrete lattice model[10] by dividing the perturbed lattice into two regions. In the near region (extended up to a few nearest neighbors surrounding the vacancy) they assumed the discrete lattice and vacancy-induced atomic displacements are taken from Singhal's calculations.[11] The far region (the remaining lattice) is assumed to be a continuum. The accuracy of the calculations depended upon the size of the near region.

A unified theory for the evaluation of the EFG requires self-consistently calculated screening charge density, interatomic potential, and the strain field. Beal-Monod and Kohn[12] made such an attempt using the asymptotic form of the charge perturbation and change in potential due to a point defect. The perturbing potential in the near region was related to the Blatt correction and in the far region to the strain field. However, the use of the asymptotic form of charge density in estimating different quantities is hardly justified near the point defect.

Recently we have evaluated the strain field due to a substitutional impurity in a cubic metal by the lattice static method[13] (referred to as paper I). The dielectric screening method is used to generate the impurity-host and host-host interatomic potentials. In this paper we generalize an internally consistent dielectric screening theory to calculate the excess potential for a substitutional impurity due to valence and size effects. These potentials are then used to compute size and valence EFGs. The calculated values explain well the experimental results of Cu and Al alloys.

The plan of the paper is as follows. The theory is presented in Sec. II. The calculations and results for Cu and Al alloys are presented in Sec. III and are discussed in Sec. IV.

II. THEORY

A. General formulation

Consider a perfect monoatomic lattice with $\mathbf{R}_n^0$ lattice points. An impurity atom is introduced at a substitution-

al (or interstitial) site assumed to be at the origin (Fig. 1). The impurity displaces the host atoms to new equilibrium positions

$$\mathbf{R}_n = \mathbf{R}_n^0 + \mathbf{u}_n \ , \tag{1}$$

where $\mathbf{u}_n$ is the displacement of the nth atom. Here the impurity is supposed to be static. If $\phi_H(\mathbf{r})$ is the self-consistent interatomic potential of the host metal, the crystal potential $\Phi_H(\mathbf{r})$, experienced by a test charge at $\mathbf{r}$ in the perfect lattice is

$$\Phi_H(\mathbf{r}) = \sum_n{}' \phi_H(\mathbf{r}-\mathbf{R}_n^0) \ , \tag{2}$$

where the dash in summation excludes the term $\mathbf{r}=\mathbf{R}_n^0$. Similarly, the crystal potential in the presence of an impurity at the origin is

$$\Phi'(\mathbf{r}) = \phi_I(\mathbf{r}) + \sum_{n(\neq 0)}{}' \phi_H(\mathbf{r}-\mathbf{R}_n) \ , \tag{3}$$

where $\phi_I(\mathbf{r})$ is the self-consistent potential due to the impurity atom. Adding and subtracting $\phi_H(\mathbf{r})$ in Eq. (3),

$$\Phi'(\mathbf{r}) = \Delta\phi(\mathbf{r}) + \Phi'_H(\mathbf{r}) \ , \tag{4}$$

where

$$\Delta\phi(\mathbf{r}) = \phi_I(\mathbf{r}) - \phi_H(\mathbf{r}) \tag{5}$$

and

$$\Phi'_H(\mathbf{r}) = \sum_n{}' \phi_H(\mathbf{r}-\mathbf{R}_n) \ . \tag{6}$$

Here $\Delta\phi(\mathbf{r})$ is the excess impurity potential and involves only the origin lattice point. Thus the total change in crystal potential due to the insertion of an impurity becomes

$$\begin{aligned}\Delta\Phi(\mathbf{r}) &= \Phi'(\mathbf{r}) - \Phi_H(\mathbf{r}) \\ &= \Delta\phi(\mathbf{r}) + \Delta\Phi_H(\mathbf{r}) \ ,\end{aligned} \tag{7}$$

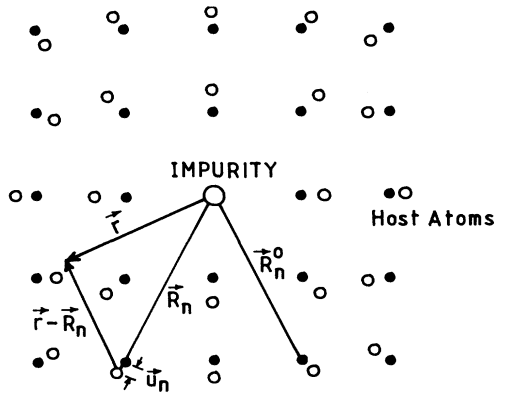

FIG. 1. Strained monoatomic lattice with substitutional impurity at the origin. The solid and open circles represent the undisplaced and the displaced positions of lattice sites, respectively.

where the strain potential

$$\begin{aligned}\Delta\Phi_H(\mathbf{r}) &= \Phi'_H(\mathbf{r}) - \Phi_H(\mathbf{r}) \\ &= \sum_n{}' [\phi_H(\mathbf{r}-\mathbf{R}_n) - \phi_H(\mathbf{r}-\mathbf{R}_n^0)] \ .\end{aligned} \tag{8}$$

From Eq. (7), it is evident that the total change in crystal potential is the sum of two distinct contributions $\Delta\phi(\mathbf{r})$ and $\Delta\Phi_H(\mathbf{r})$. $\Delta\phi(\mathbf{r})$ arises from the valence difference. It explicitly depends on the bare host ion and bare impurity ion potential and dielectric screening due to the conduction electrons. It involves only one host and one impurity atom. $\Delta\Phi_H(\mathbf{r})$ arises from the lattice strain field and involves the entire lattice.

The EFG tensor $\underset{\sim}{V}$, at $\mathbf{r}=\mathbf{R}_m$, the mth nearest neighbor (mNN) of impurity, is obtained by computing the second derivative of $\Delta\Phi(\mathbf{r})$ and is given as

$$\underset{\sim}{V}(\mathbf{R}_m) = \underset{\sim}{V}^v(\mathbf{R}_m) + \underset{\sim}{V}^s(\mathbf{R}_m) \ , \tag{9}$$

where valence EFG

$$\underset{\sim}{V}^v(\mathbf{R}_m) = (1-\gamma_\infty)\{\nabla\cdot\nabla[\Delta\phi(\mathbf{r})]\}_{\mathbf{r}=\mathbf{R}_m} \tag{10}$$

and size EFG

$$\underset{\sim}{V}^s(\mathbf{R}_m) = (1-\gamma_\infty)\{\nabla\cdot\nabla[\Delta\Phi_H(\mathbf{r})]\}_{\mathbf{r}=\mathbf{R}_m} \ . \tag{11}$$

$(1-\gamma_\infty)$ is Sternheimer antishielding factor. In principle, γ depends upon $\mathbf{r}$; however, it is found that spatial dependence is significant only in the distances less than the 1NN and then it reaches a constant value γ_∞.[14] As the EFGs are evaluated at the 1NN site and beyond, the use of γ_∞ in place of $\gamma(\mathbf{r})$ is fairly justified. Equations (10) and (11) are general equations for the valence and the size EFGs.

B. Valence EFG

The valence EFG $\underset{\sim}{V}^v(\mathbf{R}_m)$ which arises from the excess potential due to the impurity atom at the origin, is expressed in Cartesian components as

$$V^v_{\alpha\beta}(\mathbf{R}_m) = (1-\gamma_\infty)\nabla_\alpha\nabla_\beta[\Delta\phi(\mathbf{r})]_{\mathbf{r}=\mathbf{R}_m} \ , \tag{12}$$

where α and $\beta(=x,y,z)$ are Cartesian coordinates. For small atomic displacements

$$V^v_{\alpha\beta}(\mathbf{R}_m) = (1-\gamma_\infty)\nabla_\alpha\nabla_\beta\{\Delta\phi(\mathbf{R}_m^0) + \mathbf{u}_m\cdot\nabla[\Delta\phi(\mathbf{R}_m^0)]\} \ , \tag{13}$$

where only the linear term in $\mathbf{u}_m$ is retained. The second term in Eq. (13) is the first-order correction and is termed as indirect size effect. The Blatt correction does not arise as the interaction between atoms is taken at their exact displaced positions.[15]

C. Size EFG

Substitution of $\Delta\Phi_H(\mathbf{r})$ from Eq. (8) in (11) gives

$$\underset{\sim}{V}^s(\mathbf{R}_m)=(1-\gamma_\infty)\left[\nabla\cdot\nabla\sum_{n(\neq m)}'\phi_H(\mathbf{r}-\mathbf{R}_n)-\nabla\cdot\nabla\sum_{n(\neq m)}'\phi_H(\mathbf{r}-\mathbf{R}_n^0)\right]_{\mathbf{r}=\mathbf{R}_m}$$
$$=(1-\gamma_\infty)\left[\nabla\cdot\nabla\sum_{n(\neq m)}'[\phi_H(\mathbf{r}-\mathbf{R}_n)-\phi_H(\mathbf{r}-\mathbf{R}_n^0)]\right]_{\mathbf{r}=\mathbf{R}_m}. \quad (14)$$

The second term involves the sum over the perfect lattice, therefore the sum of derivatives vanishes due to cubic symmetry. Thus for a cubic lattice

$$\underset{\sim}{V}^s(\mathbf{R}_m)=(1-\gamma_\infty)\nabla\cdot\nabla\sum_{n(\neq m)}'\phi_H(\mathbf{r}-\mathbf{R}_n)\Big|_{\mathbf{r}=\mathbf{R}_m}. \quad (15)$$

The Cartesian components of the size EFG tensor are

$$V^s_{\alpha\beta}(\mathbf{R}_m)=(1-\gamma_\infty)\nabla_\alpha\nabla_\beta\sum_{n(\neq m)}'\phi_H(\mathbf{r}-\mathbf{R}_n)\Big|_{\mathbf{r}=\mathbf{R}_m}. \quad (16)$$

Equation (16) is a general expression for $\underset{\sim}{V}^s(\mathbf{R}_m)$ for a cubic crystal which can be evaluated if the self-consistent interatomic potential of the host lattice is known.

If we assume the lattice ions as point charges[16] which interact through Coulomb potential, Eq. (16) gets simplified as

$$V^s_{\alpha\beta}(\mathbf{R}_m)=(1-\gamma_\infty)\nabla_\alpha\nabla_\beta\sum_{n(\neq m)}'\frac{Z_He}{|\mathbf{r}-\mathbf{R}_n|}\Big|_{\mathbf{r}=\mathbf{R}_m}. \quad (17)$$

Equation (17) was used by Hafizuddin and Mohapatra[8] to calculate the size EFG. $\phi_H(\mathbf{r}-\mathbf{R}_n)$ in Eq. (16) is expanded in powers of u_n and, retaining only the linear term, one finds

$$V^s(\mathbf{R}_m)=(1-\gamma_\infty)\nabla_\alpha\nabla_\beta\sum_{n(\neq m)}[\hat{u}(\mathbf{R}_m^0-\mathbf{R}_n)]\cdot[\nabla\phi_H(\mathbf{R}_m^0-\mathbf{R}_n^0)]$$
$$=(1-\gamma_\infty)\nabla_\alpha\nabla_\beta\sum_{n(\neq m)}\mathbf{u}_n\cdot\nabla\phi(\mathbf{R}_m^0-\mathbf{R}_n^0). \quad (18)$$

Here we used the fact that $V^s_{\alpha\beta}(\mathbf{R}_m)$ vanishes for a perfect cubic crystal. Sagalyn and co-workers[4,9] suggested a relation equivalent to Eq. (18) for the continuum model of the lattice to evaluate the size EFG and the same expression was later used by many other authors[2] by introducing different nature of size strength parameters. Beal-Monod and Kohn[12] also used a similar relation for the evaluation of the size EFG. Equation (14) involves the complete $\phi_H(\mathbf{r}-\mathbf{R}_n)$ while Eq. (18) consists of the expansion of $\phi_H(\mathbf{r}-\mathbf{R}_n)$ only up to first order. Again for the fast convergence Eq. (14) rather than Eq. (16) is used to evaluate size EFGs.

D. Addition of valence and size EFGs

The total EFG is obtained from Eq. (9) by adding the corresponding components of valence and size effect EFGs, i.e.,

$$V_{\alpha\beta}(\mathbf{R}_m)=V^v_{\alpha\beta}(\mathbf{R}_m)+V^s_{\alpha\beta}(\mathbf{R}_m). \quad (19)$$

The components of traceless EFG tensor $\underset{\sim}{q}$ are given as

$$q_{\alpha\beta}=V_{\alpha\beta}-\frac{1}{3}\sum_\alpha V_{\alpha\alpha}. \quad (20)$$

The (3×3) matrix of $q_{\alpha\beta}$ is diagonalized to obtain the eigenvalues and eigenvectors. The eigenvalue corresponding to the eigenvector parallel to the line joining the impurity and the host atom is taken as

$$q_{zz}=q_\parallel. \quad (21)$$

Other two components are written as

$$q_{yy}=q_\perp,\quad q_{XX}=q_{xx}. \quad (22)$$

In general, $|q_{zz}|\geq|q_{yy}|\geq|q_{XX}|$. The asymmetry parameter is defined as

$$\eta=|q_{XX}-q_{yy}|/|q_{zz}|. \quad (23)$$

In the fcc lattice $\underset{\sim}{V}^v$ and $\underset{\sim}{V}^s$ are similar matrices at the 1NN and 2NNs. Therefore, these can be diagonalized separately and eigenvalues obtained can be added for the same eigenvectors. However, this may not be the situation at the 3NNs.

III. CALCULATIONS AND RESULTS

A. The scattering potential $\Delta\phi(\mathbf{r})$

In a metal, the ions are embedded in a uniform or nonuniform sea of conduction electrons which screen the electron-ion interaction. The point ion approximation is also not appropriate as the cores have finite size and potential is repulsive in this region. The pseudopotentials include these effects and are well established for the simple metals.[15,17] Therefore, we used the screened pseudopotentials for electron-ion interaction in metallic alloys.[18] Further, it is assumed that the electron density remains practically the same in the defect lattice as in the perfect lattice. Therefore, both the impurity and the host bare-

ion potentials are screened by the same dielectric function of the host metal.

It is more convenient to evaluate $\Delta\phi(\mathbf{r})$ in the Fourier space. Equation (5) in Fourier space can be written as

$$\Delta\phi(\mathbf{q})=\phi_I(\mathbf{q})-\phi_H(\mathbf{q}) , \tag{24}$$

where $\mathbf{q}$ is a wave vector in Fourier space. As the bare-ion impurity and host potentials $\phi_I^b(\mathbf{q})$ and $\phi_H^b(\mathbf{q})$ both are screened by the dielectric function $\epsilon_H(\mathbf{q},\mathbf{q}')$ of the host,[18]

$$\Delta\phi(\mathbf{q})=\sum_{\mathbf{q}'}\epsilon_H^{-1}(\mathbf{q},\mathbf{q}')\Delta\phi^b(\mathbf{q}') , \tag{25}$$

where

$$\Delta\phi^b(\mathbf{q})=\phi_I^b(\mathbf{q})-\phi_H^b(\mathbf{q}) . \tag{26}$$

For the nearly free-electron metals like Cu and Al, the dielectric matrix is almost diagonal, i.e.,

$$\epsilon_H(\mathbf{q},\mathbf{q}')=\epsilon_H(\mathbf{q})\delta\mathbf{q}\mathbf{q}' .$$

Therefore,

$$\Delta\phi(\mathbf{q})=\Delta\phi^b(\mathbf{q})/\epsilon_H(\mathbf{q}) . \tag{27}$$

We use the Ashcroft model potential for $\phi_I^b(\mathbf{q})$ and $\phi_H^b(\mathbf{q})$ whose Fourier transform is

$$\phi^b(q)=-(4\pi Ze^2/q^2)\cos(qr_c) , \tag{28}$$

where r_c is the model potential parameter and represents effective core radius. The Hartree dielectric function modified by Hubbard exchange-correlation corrections $f_{xc}(\mathbf{q})$ (Ref. 19) is used for $\epsilon_H(\mathbf{q})$. Explicitly

$$\epsilon_H(\mathbf{q})=1+\frac{me^2}{\pi\hbar^2\zeta^2k_f}[1-f_{xc}(\mathbf{q})] \times\left[\frac{1}{2}+\frac{1-\zeta^2}{4\zeta}\ln\left|\frac{1+\zeta}{1-\zeta}\right|\right] , \tag{29}$$

where $\zeta=q/2k_f$. k_f, e, and m are Fermi wave vector, electronic charge, and mass, respectively. One can also use $f_{xc}(\mathbf{q})$ suggested by Geldart and Vosko[20] and Vashishta and Singwi[21] which are obtained by satisfying the compressibility sum rule. The effect of exchange-correlation corrections is explicitly investigated in the calculations of phonon frequencies and other related properties.[22] However, in the present investigations of electric-field gradients, other approximations are more vital; therefore, for simplicity, we used $f_{xc}(\mathbf{q})$ as did Hubbard.[19]

From Eq. (27) $\Delta\phi(\mathbf{r})$ is obtained as

$$\Delta\phi(\mathbf{r})=\frac{1}{(2\pi)^3}\int\frac{\Delta\phi^b(\mathbf{q})}{\epsilon_H(\mathbf{q})}e^{i\mathbf{q}\cdot\mathbf{r}}d\mathbf{q} . \tag{30}$$

Use of Eq. (28) for the host and impurity bare-ion potentials in Eq. (30) leads to

$$\Delta\phi(r)=-\frac{2e^2}{\pi}\int\left[\frac{\Delta Z}{\epsilon_H(q)}\cos(qr_{cH}) +\frac{Z_I}{\epsilon_H(q)}(\cos qr_{cI}-\cos qr_{cH})\right] \times(\sin qr/qr)dq . \tag{31}$$

Here Z_I and Z_H are the impurity and host valencies, r_{cI} and r_{cH} are corresponding potential parameters, and $\Delta Z=Z_I-Z_H$ denotes the excess impurity charge. Equation (31) is evaluated numerically by multiplying it by the damping factor

$$\exp[-0.03(q/2k_f)^4]$$

for convergence.[17] As $\epsilon_H(q)$ in Eq. (29) is isotropic, $\Delta\phi(\mathbf{r})$ is also isotropic. The variation of $\Delta\phi(\mathbf{r})$ with $\mathbf{r}$ for *Cu*(Mg,Zn,Sn) and *Al*(Mg,Zn,Sn) is shown in Figs. 2 and 3, respectively, and the parameters used are tabulated in Table I.

For the Ashcroft model potential we write the difference in bare-ion potentials as

$$\phi_I^b(r)-\phi_H^b(r)=e^2(\Delta Z/r) -e^2(1/r)[Z_I\Theta(r_{cI}-r) -Z_H\Theta(r_{cH}-r)] . \tag{32}$$

The right-hand side depends only on ΔZ for $r>r_{cI},r_{cH}$; however, for $r<r_{cI},r_{cH}$ it is nonunique and sensitive to

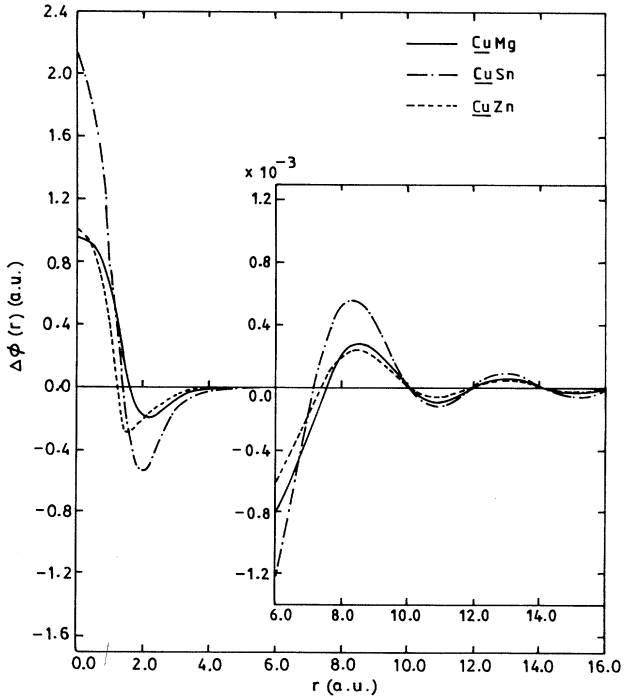

FIG. 2. $\Delta\phi(r)$ vs r for *Cu* alloys. The solid lines, dash-dot lines and dashed lines are for *Cu*Mg, *Cu*Sn, and *Cu*Zn alloys, respectively.

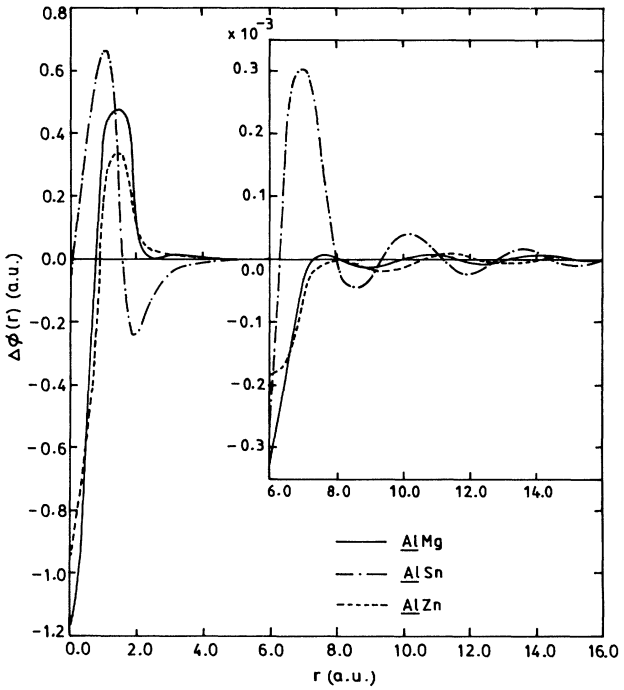

FIG. 3. $\Delta\phi(r)$ vs r for Al alloys. The solid lines, dash-dot lines, and dashed lines are for AlMg, AlSn, and AlZn alloys, respectively.

relative magnitudes of r_{cI} and r_{cH}. The same characteristics are involved in $\Delta\phi(r)$ given in Eq. (31). The calculations show that in Cu alloys, the host potential is larger than the impurity potential in the vicinity of impurity while it is the reverse for Al alloys. Consequently, the electron charge density depletes in Cu alloys in the impurity cell while it increases in Al alloys.[23]

In Cu alloys the potentials are maximum at the impurity site, they decrease rapidly away from the impurity, and show the oscillatory nature at large distances. The $\Delta\phi(0)$ is maximum for CuSn as ΔZ is maximum. The small difference in $\Delta\phi(0)$ for CuZn and CuMg is due to the second term in Eq. (31). The relative strength of $\Delta\phi(\mathbf{r})$ is in accordance with ΔZ and potential parameters. The first potential minimum is at about 2 a.u. which is less than half the distance of the first nearest neighbor of impurities for all the alloys. Therefore, the maximum depletion in electronic charge density is at impurity site and maximum pileup at about half of the 1NN distance of the impurity. At the displaced positions of the 1NN of CuMg (5.12 a.u.), CuZn (5.09 a.u.), and CuSn (5.24 a.u.) the potentials are attractive; therefore, the pileup of charge density exists. A similar comment is also valid for displaced 2NN positions. However, if the potential is repulsive at any displaced NN site, depletion in charge density will exist.

TABLE I. The physical parameters (in a.u.) of Al, Cu, Mg, Zn, and Sn elements. a is lattice constant, k_f is Fermi momentum, Z is valency, and r_c are potential parameters.

	Al	Cu	Mg	Zn	Sn
a	7.637	6.834			
k_f	0.927	0.720			
Z	3	1	2	2	4
r_c	1.12	0.81	1.39	1.27	1.30

The similar behavior of $\Delta\phi(r)$ vs r is found for Al(Mg,Zn,Sn) alloys except that $\Delta\phi(r)$ is negative in the vicinity of the impurities. The first minima of the potential is at about 1 a.u. from the impurity in AlSn while at about 1.5 a.u. in AlMg and AlZn. For larger r, $\Delta\phi(r)$ is oscillatory. The $\Delta\phi(r)$ at the displaced 1NN position is attractive for Al(Mg,Zn,Sn) alloys while at the 2NN it is attractive for Al(Mg,SN) and repulsive for AlZn.

The intercomparison for Al and Cu host metals with the same impurities shows that $\Delta\phi(r)$ in case of Cu is larger in magnitude than that for Al which may be attributed to the larger screening effects (larger conduction electron density) in Al metal. The over all results for $\Delta\phi(r)$ show that these depend on the magnitude of ΔZ and the effective core radii. This becomes evident from the fact that ΔZ is positive for Sn impurity in Al but $\Delta\phi(r)$ exhibits a very small negative value at $r=0$.

B. The strain field

To study the strain potentials $\Delta\Phi_H(\mathbf{r})$ given in Eq. (8) the two-body interatomic potential $\phi_H(\mathbf{r})$ for perfect and strained lattice is taken the same as in paper I for internal consistency of calculations. It is assumed that the functional form of $\phi_H(\mathbf{r})$ remains unaltered for perfect and strained lattices. The use of Ashcroft potential for bare ions and $\epsilon_H(\mathbf{q})$ given in Eq. (29) yields the crystal potential of the strained lattice given in Eq. (6) experienced by a test charge at $\mathbf{r}$ as

$$\Phi'_H(\mathbf{r})=\sum_n{}' \left[\frac{Z_H e}{|\mathbf{r}-\mathbf{R}_n|}+\frac{2Z_H e}{\pi}\int dq \left[\frac{1}{\epsilon(q)}-1\right]\cos^2 q r_{cH}\frac{\sin q(|\mathbf{r}-\mathbf{R}_n|)}{q(|\mathbf{r}-\mathbf{R}_n|)}\right]. \tag{33}$$

The first term in Eq. (33) is the Coulomb interaction due to ions and the second term represents the interaction due to ions via conduction electrons. The corresponding potential in the perfect lattice $\Phi_H(\mathbf{r})$ given in Eq. (2) is obtained by replacing $\mathbf{R}_n$ with $\mathbf{R}_n^0$ in Eq. (33). Thus

$$\Delta\Phi_H(\mathbf{r})=\sum_n{}' \left[Z_H e\left[\frac{1}{|\mathbf{r}-\mathbf{R}_n|}-\frac{1}{|\mathbf{r}-\mathbf{R}_n^0|}\right]+\frac{2Z_H e}{\pi}\int dq[\epsilon_H^{-1}(q)-1]\cos^2 q r_{cH}\left[\frac{\sin q(|\mathbf{r}-\mathbf{R}_n|)}{q(|\mathbf{r}-\mathbf{R}_n|)}-\frac{\sin q(|\mathbf{r}-\mathbf{R}_n^0|)}{q(|\mathbf{r}-\mathbf{R}_n^0|)}\right]\right]. \tag{34}$$

Both the terms $\mathbf{r}=\mathbf{R}_n$ and $\mathbf{r}=\mathbf{R}_n^0$ are excluded. The $\Delta\Phi_H(\mathbf{r})$ is anisotropic and follows the crystal symmetry.

We calculated $\Phi_H(\mathbf{r})$ and $\Delta\Phi_H(\mathbf{r})$ along principal symmetry directions [001], [011], and [111]. $\Phi'_H(\mathbf{r})$ is too close to $\Phi_H(\mathbf{r})$ on the same scale. The quadrature method is used for numerical integration. Because of the Coulomb term the integral converged up to $q=10$ (a.u.)$^{-1}$. For sum over n, the fcc crystallite was generated up to 28NNs amounting to 958 atoms. The tables of lattice displacements reported in paper I were extended and used in Eq. (34). It is found that the variation in $\Delta\Phi_H(\mathbf{r})$ is of the order of 10^{-5} a.u. beyond 14 neighbors in Cu ($|\mathbf{r}-\mathbf{R}_n^0|\cong 17$ a.u.) and Al ($|\mathbf{r}-\mathbf{R}_n^0|\cong 18$ a.u.) This is equivalent to the sum over about 250 atoms in Cu alloys and 200 atoms in Al alloys. This criterion was followed at each $\mathbf{r}$ at different distances from the defect center. At large $\mathbf{r}$ the sum over n converged even for less number of NNs due to smaller displacements. For $\Phi_H(\mathbf{r})$ the sum over n is taken up to 20 NNs due to smaller displacements.

The results for $\Phi_H(\mathbf{r})$ and $\Delta\Phi_H(\mathbf{r})$ for *Cu*(Mg,Zn,Sn) and *Al*(Mg,Zn,Sn) are shown in Figs. 4–9 along principal symmetry directions. The following observations are made.

(i) The crystal potential $\Phi_H(\mathbf{r})$ shown by dash-cross lines is periodic. The periodicity is a, $a\sqrt{2}$, and $a\sqrt{3}$ along [001], [011], and [111] directions respectively. The presence of face atoms along [111] direction is evident from the two broad maxima in $\Phi_H(\mathbf{r})$ along [111] direction. The potentials are singular at atomic sites. Our choice of $\phi_H(\mathbf{r})$ kept $\Phi_H(\mathbf{r})$ repulsive along all the three directions for both the metals. $\Phi_H(\mathbf{r})$ can be made zero or even negative by an appropriate choice of $\phi_H(\mathbf{r})$.[24]

(ii) $\Delta\Phi_H(\mathbf{r})$ is calculated up to $r=13.67$, 19.33, and 23.67 a.u. along [001], [011], and [111] directions in Cu alloys. The corresponding distances in Al alloys are 15.27, 21.59, and 26.45 a.u. The $|\Delta\Phi_H(\mathbf{r})|$ is larger by an order of magnitude along [011] as compared to that along [001] and [111] directions. Along [001] and [111] directions $|\Delta\Phi_H(\mathbf{r})|$ is comparable. Evidently, the larger the atomic density is in a particular direction, the larger $|\Delta\Phi_H(\mathbf{r})|$ is.

(iii) In the Cu alloys, ΔZ is positive for all the impurities; consequently, $\Delta\Phi_H(\mathbf{r})$ is similar for all the alloys. In Al alloys ΔZ is positive for Sn and negative for Mg and Zn impurities; therefore, the spatial variation of $\Delta\Phi_H(\mathbf{r})$ for *Al*Sn is different from those of *Al*(Mg,Zn). Further, the larger the ΔZ, the larger $\Delta\Phi_H(r)$ is. The nature of $\Delta\Phi_H(\mathbf{r})$ changes from period to period in the different directions and it is also oscillatory in the same period. This is due to different pattern of atomic displacements and atomic arrangement of nearest neighbors in different directions. Thus $\Delta\Phi_H(\mathbf{r})$ implicitly depends on $\phi_H(\mathbf{r}),\phi_I(\mathbf{r})$ and is very sensitive to the atomic displacements.

(iv) In the vicinity of lattice sites, $\Delta\Phi_H(\mathbf{r})$ is large as it is the difference of two large quantities. In between the lattice sites $|\Delta\Phi_H(\mathbf{r})|$ decreases with increase in distance from the defect site. This fact is more explicit in the Al alloys. It is found that $\Delta\Phi_H(\mathbf{r})$ in the intermediate region becomes negligibly small beyond 600 atoms. Therefore, a crystallite of this size may be quite appropriate, but this size may change with the choice of $\phi_H(\mathbf{r})$ and $\phi_I(\mathbf{r})$.

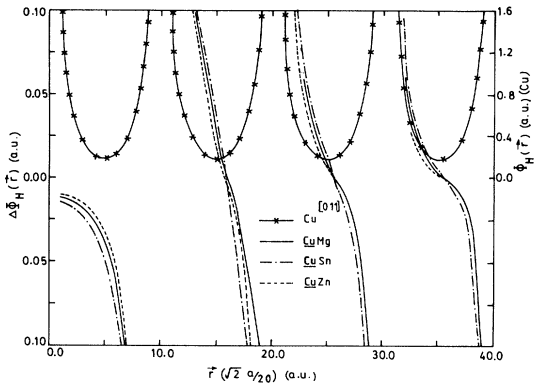

FIG. 5. $\Phi_H(\mathbf{r})$ and $\Delta\Phi_H(\mathbf{r})$ vs $\mathbf{r}$ for Cu and Cu alloys along the [011] direction. $\mathbf{r}$ is in units of $(\sqrt{2}a/20)$ a.u. At large distances, the dashed line coincides with solid line.

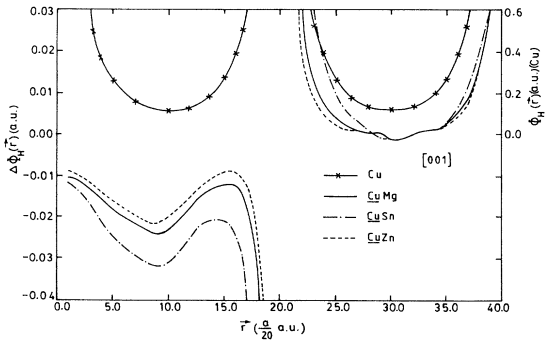

FIG. 4. $\Phi_H(\mathbf{r})$ and $\Delta\Phi_H(\mathbf{r})$ vs $\mathbf{r}$ for Cu and Cu alloys along the [001] direction. $\mathbf{r}$ is in units of $(a/20)$ a.u.

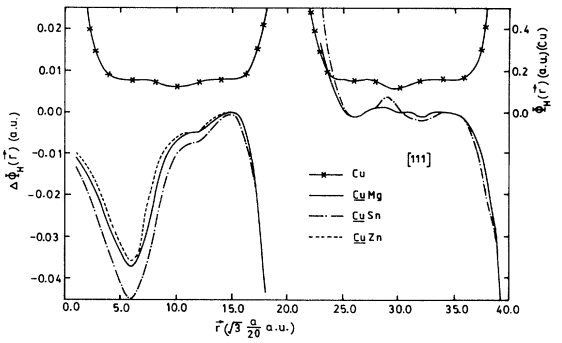

FIG. 6. $\Phi_H(\mathbf{r})$ and $\Delta\Phi_H(\mathbf{r})$ vs $\mathbf{r}$ for Cu and Cu alloys along the [111] direction. $\mathbf{r}$ is in units of $(\sqrt{3}a/20)$ a.u. At large distances, the dashed line coincides with the solid line.

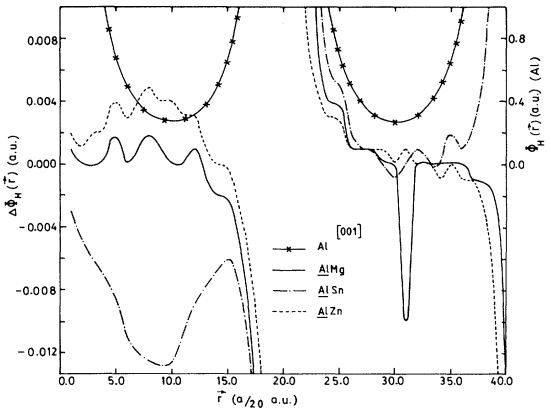

FIG. 7. $\Phi_H(\mathbf{r})$ and $\Delta\Phi_H(\mathbf{r})$ vs $\mathbf{r}$ for Al and Al alloys along the [001] direction. $\mathbf{r}$ is in units of $(a/20)$ a.u.

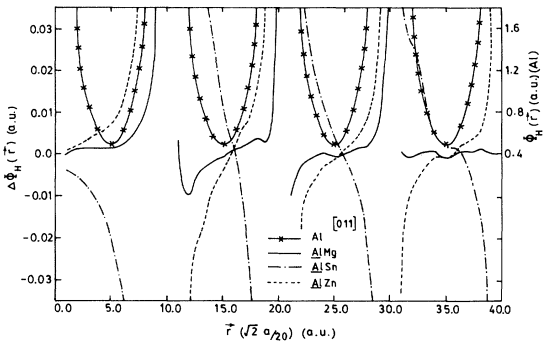

FIG. 8. $\Phi_H(\mathbf{r})$ and $\Delta\Phi_H(\mathbf{r})$ vs $\mathbf{r}$ for Al and Al alloys along the [011] direction. $\mathbf{r}$ is in units of $(\sqrt{2}a/20)$ a.u.

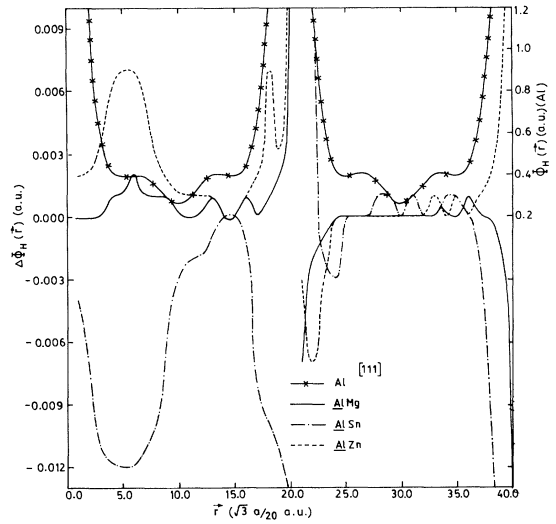

FIG. 9. $\Phi_H(\mathbf{r})$ and $\Delta\Phi_H(\mathbf{r})$ vs $\mathbf{r}$ for Al and Al alloys along the [111] direction. $\mathbf{r}$ is in units of $(\sqrt{3}a/20)$ a.u.

C. The electric-field gradients

The impurity induced change in potential $\Delta\phi(r)$ given in Eq. (31) is used in Eq. (12) to evaluate $V^v_{\alpha\beta}$. The differentiation is carried out numerically at the displaced positions of 1NN and 2NNs of impurities. These values are used in Eq. (20) to get the traceless EFG components $q^v_{\alpha\beta}$. Similarly, the strain potential $\Delta\Phi_H(\mathbf{r})$ given in Eq. (34) is used in Eq. (11) to obtain $V^s_{\alpha\beta}(\mathbf{R}_m)$ at the displaced positions and finally in Eq. (20) to get $q^s_{\alpha\beta}$. In Eq. (34) the sum over n is carried out up to 14NNs of the point of observation $\mathbf{R}_m$ to achieve the convergence within the limits of accuracy for both the Cu and Al alloys.

At both the 1NN and 2NN $\underset{\sim}{q}^v$ and $\underset{\sim}{q}^s$ matrices are similar. Their eigenvectors are found parallel and corresponding eigenvalues are added. The same answer is obtained by first adding the components of $\underset{\sim}{q}^v$ and $\underset{\sim}{q}^s$ and then diagonalizing the resulting matrix. At the 1NN site, the nonzero components are $q^{v(s)}_{xx}$, $q^{v(s)}_{yy}$, $q^{v(s)}_{zz}$, $q^{v(s)}_{yz}$. The eigenvectors are [100], [0$\bar{1}$1], and [011] and the corresponding eigenvalues are $q^{v(s)}_{xx}$, $q^{v(s)}_{\perp}$, and $q^{v(s)}_{\parallel}$. The EFG is evaluated at the displaced $(a/2)(011)$ atom. At the 2NN site the $\underset{\sim}{q}^{v(s)}$ is diagonal. The eigenvectors are [100], [010], and [001]. The corresponding eigenvalues are $q^{v(s)}_{xx}$, $q^{v(s)}_{\perp}$, and $q^{v(s)}_{\parallel}$. The EFG is evaluated at the displaced $(a/2)(002)$ atom. These values are tabulated in Tables II and III for Cu and Al alloys. The resulting EFGs and asymmetry parameter η are also tabulated there.

In these calculations the antishielding factor $(1-\gamma_\infty)$ is known with the least accuracy. It is shown by Pattnaik, Thompson, and Das[25] that exchange-correlation interactions between core and conduction electrons greatly affect γ_∞. But the accurate estimation of these interactions is too difficult. Conventionally,[26] $(1-\gamma_\infty)$ is taken to be 18.36, 3.59, and 12.0 for Cu, Al, and V alloys, respectively. However, in these calculations[4–9] the size parameter has been arbitrary. Sagalyn and Alexander[9] pointed out that in the absence of screening, $(1-\gamma_\infty)\cong R_0^3$ (R_0 is 1NN distance). This estimation is nearly valid for Cu and V; it is too low, however, for Al.

We used $(1-\gamma_\infty)=18.36$ for Cu alloys. The calculated values of EFG and η are found in good agreement with the experimental values. These calculations do not involve arbitrary core enhancement factor and size strength parameter. However, for Al alloys with $(1-\gamma_\infty)=3.59$ the calculated results were found smaller than the experimental values by an order of magnitude. Therefore, we used

$$(1-\gamma_\infty)=23.37(\cong R_0^3)$$

for Al alloys which yielded good agreement with the experimental values.

We notice from Tables II and III that the size EFG components at the 1NN have cubic symmetry while valence EFG components have cylindrical symmetry. This is due to the fact that $\Delta\Phi_H(\mathbf{r})$ has the crystal symmetry while $\Delta\phi(\mathbf{r})$ is spherically symmetric. At the 2NN both the valence and size EFGs are cylindrically sym-

TABLE II. The calculated and the experimental values of EFG (in A^{0-3}) and asymmetry parameter η at the 1NN and 2NNs of Mg, Zn, and Sn impurities in *Cu*. The η vanishes at the 2NN site.

Impurity	EFG contribution	q_{xx}	$q_{\perp}$	$q_{\parallel}$	$\lvert q\rvert_{cal}$ [expt.]	η_{cal} [expt.]
			(1NN)			
Mg	Valence	0.3308	0.3308	−0.6616	0.77	0.21
	Size	−0.0257	0.1352	−0.1096		
	Total	0.3050	0.4660	−0.7712		
Zn	Valence	0.271	0.271	−0.542	0.64	0.23
	Size	−0.025	0.125	−0.099	[0.71]	[0.27]
	Total	0.246	0.396	−0.641		
Sn	Valence	0.481	0.481	−0.963	1.109	0.17
	Size	−0.024	0.170	−0.146	[0.85]	[0.63]
	Total	0.457	0.651	−1.109		
			(2NN)			
Mg	Valence	−0.0041	−0.0041	0.0083	0.0786	
	Size	0.0434	0.0434	−0.0868		
	Total	0.0393	0.0393	−0.0785		
Zn	Valence	−0.00013	−0.00013	0.0003	0.076	
	Size	0.0384	0.0384	−0.0768	[< 0.3]	
	Total	0.0383	0.0383	−0.0765		
Sn	Valence	0.0161	0.0161	−0.0322	0.154	
	Size	0.0607	0.0607	−0.1215	[0.42]	
	Total	0.0768	0.0768	−0.1537		

TABLE III. The calculated and experimental values of EFG (A^{0-3}) and asymmetry parameter η at the 1NN and 2NNs of Mg, Zn, and Sn impurities in *Al*. The η vanishes at the 2NN site.

Impurity	EFG contribution	q_{xx}	$q_{\perp}$	$q_{\parallel}$	$\lvert q\rvert_{cal}$ [expt.]	η_{cal} (η_{expt})
			(1NN)			
Mg	Valence	−0.043	−0.043	0.086	0.095	0.27
	Size	0.008	−0.018	0.009	[0.195]	[0.07]
	Total	−0.035	−0.061	0.095		
Zn	Valence	−0.058	−0.058	0.116	0.13	0.39
	Size	0.017	−0.035	0.018	[0.18]	[0.27]
	Total	−0.041	−0.093	0.134		
Sn	Valence	0.083	0.083	−0.167	0.21	0.46
	Size	−0.028	0.067	−0.038	[0.27]	[0.37]
	Total	0.055	0.150	−0.205		
			(2NN)			
Mg	Valence	0.0109	0.0109	−0.0218	0.023	
	Size	0.0004	0.0004	−0.0008	[< 0.02]	
	Total	0.0113	0.0113	−0.0226		
Zn	Valence	0.0087	0.0087	−0.0175	0.012	
	Size	−0.0026	−0.0026	0.0052	[< 0.02]	
	Total	0.0061	0.0061	−0.0123		
Sn	Valence	−0.0045	−0.0045	0.0091	0.015	
	Size	0.0121	0.0121	−0.0242	[0.049]	
	Total	0.0076	0.0076	−0.0151		

metric. If the effect of quasilocalized electrons is included through the nondiagonal part of the dielectric matrix[27] the symmetry of $\Delta\phi(\mathbf{r})$ and hence that of q^v will also change. Thus the EFG components are sensitive to the symmetries of the potentials used for their evaluation.

For all the Cu and Al alloys at the 1NN site, $|q^v_{\parallel}| > |q^v_{\perp}| = |q^v_{xx}|$ while $|q^s_{\perp}| > |q^s_{\parallel}| > |q^s_{xx}|$. At the 2NN, $|q^v_{\parallel}| > |q^v_{\perp}| = |q^v_{xx}|$ and $|q^s_{\parallel}| > |q^s_{\perp}| = |q^s_{xx}|$ for all the Cu and Al alloys. At the 1NN $|q^v_{\rm cal}|$ is larger than $|q^s_{\rm cal}|$ even componentwise for all the Cu and Al alloys. But at 2NNs, $|q^s_{\rm cal}|$ is larger by an order of magnitude than $|q^v_{\rm cal}|$ for Cu alloys while reverse is true in Al alloys.

At the 1NN site $|q^v_{\rm cal}|$ in the Cu alloys are larger than in the Al alloys. This depended on both ΔZ and the potential parameters r_{cI} and r_{cH}. Again due to larger displacements, $|q^s_{\rm cal}|$ is larger in the Cu alloys than in the Al alloys. Relative comparison shows that $|q^s_{\rm cal}|$ does not depend explicitly upon ΔZ. At the 2NN site, $|q^v_{\rm cal}|$ for *Cu*Mg and *Cu*Zn are smaller than $|q^v_{\rm cal}|$ for *Al*Mg and *Al*Zn alloys. However, $|q^v_{\rm cal}|$ for *Cu*Sn is larger than that for *Al*Sn alloy. This is due to the larger ΔZ for *Cu*Sn than for the *Al*Sn alloy. $|q^s_{\rm cal}|$ for Cu alloys are larger than those for Al alloys due to larger atomic displacements in Cu alloys.

Keeping in view the uncertainties in the estimation of the $|q_{\rm exp}|$ and η from the measured data,[28] we conclude that our $|q_{\rm cal}|$ and $\eta_{\rm cal}$ agree well with $|q_{\rm exp}|$ and $\eta_{\rm exp}$. The theory is without any adjustable size strength parameter. The deviations in the calculated and the experimental values in the *Cu*Sn at the 2NN site and in the *Al*Mg at the 1NN site can be further minimized by replacing Ashcroft model potential by a more appropriate potential and also by refining the experiments.

In the calculations of Hafizuddin and Mohapatra[8] for *Al*-vac and *Cu*-vac, the magnitudes of valence EFG are larger than those of size EFG up to 4NNs while in our calculations, the size EFG becomes larger at large distances. This is an expected result as valence perturbation is larger for a vacancy than for a substitutional defect. In all other calculations[28] the size EFG is multiplied by an adjustable parameter; therefore, a direct comparison with our results is not possible.

IV. DISCUSSION

In this paper, we have presented a theory for direct calculation of EFG from the first principles. The impurity-induced scattering potential and strain potentials are calculated using linear screening theory. The nondiagonal part of dielectric matrix which arises due to partial localization of conduction electrons is neglected.[27] This approximation is fairly valid for Al alloys. However, in Cu, *d* bands are narrow and well below the fermi surface; therefore, these effects may not be dominant.

The theory is free from arbitrary size strength parameter. The uncertainties such as in the charge density in the asymptotic and preasymptotic regions and the core-enhancement factors involved in the partial-wave analysis[4–9] no longer exist. The scattering potential is also not parametrized.[8] The established pseudopotentials which have reproduced other physical properties of Cu and Al are used.

Here the valence and size EFGs are calculated in an internally consistent manner. The discrete lattice model is used for the calculation of both the valence and size EFGs. The same potential is used to compute the atomic displacements and the EFG. The sum over the NNs of impurity is carried out to the far distances to ensure the convergence of the potential and its derivatives. In the elastic continuum model, such calculations are inconsistent. The parameter used in our theory is Sternheimer antishielding factor. The estimation of these parameters in the solid phase is itself a difficult problem. However, the reasonably known values of $(1-\gamma_\infty)$ are found useful.

In the present calculations, the two-body potential is calculated using dielectric response theory. In fact, the calculations of local microfields are carried out entirely within one electron approximation. The exchange-correlation interaction among electrons are included only through the factor $f_{\rm xc}(\mathbf{q})$. The results can be improved by a better choice of a bare electron-ion potential and including nonlinear effects in the dielectric function. Other methods can also be adopted to calculate $\phi(r)$. In conclusion, we have presented an internally consistent theory of EFG where the discrete lattice model is used throughout. From the agreement between the calculated and the experimental values of q and η, we can say that the EFGs are fairly understood at least in simple metal alloys.

ACKNOWLEDGMENTS

The financial assistance from University Grants Commission, New Delhi and Department of Atomic Energy, Bombay is gratefully acknowledged.

[1]G. Grüner and M. Minier, Adv. Phys. **26**, 231 (1977).
[2]S. Prakash, Hyperfine Interaction **24**, 491 (1985).
[3]W. Kohn and S. H. Vosko, Phys. Rev. **119**, 912 (1960); A. Blandin and J. Friedel, J. Phys. Radium **21**, 689 (1960).
[4]P. L. Sagalyn, A. Paskin, and R. J. Harrison, Phys. Rev. **124**, 428 (1961).
[5]S. D. Raj, J. Singh, and S. Prakash, J. Phys. F **12**, 1941 (1982).
[6]M. J. Ponnabalam and P. Jena, Phys. Rev. Lett. **46**, 610 (1981); Solid State Commun. **52**, 411 (1984).
[7]B. Pal, S. Mahajan, S. D. Raj, J. Singh, and S. Prakash, Phys. Rev. B **30**, 3191 (1984).
[8]S. Hafizuddin and N. C. Mohapatra, J. Phys. F **16**, 217 (1986).
[9]P. L. Sagalyn and M. N. Alexander, Phys. Rev. B **15**, 5581 (1977).
[10]P. T. Heald, in *Vacancies 76* (The Metal Society, Bristol, 1977), p. 11.
[11]S. P. Singhal, Phys. Rev. B **8**, 3641 (1973).
[12]M. T. Beal-Monod and W. Kohn, J. Phys. Chem. Solids **29**, 1877 (1968).
[13]S. K. Rattan, P. Singh, S. Prakash, and J. Singh, Phys. Rev. B **47**, 599 (1993), paper I.
[14]M. H. Cohen and F. Rief, *Solid State Physics* (Academic, New

York, 1957), Vol. 5, p. 321.
[15]W. A. Harrison, *Pseudopotentials in the Theory of Metals* (Benjamin, New York, 1966).
[16]E. A. Faulkner, Philos. Mag. **5**, 843 (1960).
[17]V. Heine, *Solid State Physics* (Academic, New York, 1970), Vol. 24, p. 1.
[18]J. Singh, S. K. Rattan, and S. Prakash, Phys. Lett. **107A**, 129 (1985).
[19]J. Hubbard, Proc. Roy. Soc. London Ser. A **243**, 336 (1957).
[20]D. J. W. Geldart and S. H. Vosko, Cand. J. Phys. **44**, 2137 (1966).
[21]P. Vashishta and K. S. Singwi, Phys. Rev. B **6**, 4883 (1972).
[22]S. Prakash, in *Current Trends in Lattice Dynamics,* edited by K. R. Rao (Indian Physics Association, Bombay, 1979), p. 197.
[23]D. Deutz, P. H. Dederichs, and R. Zeller, J. Phys. F **11**, 1787 (1981).
[24]Neil W. Ashcroft and N. David Mermin, *Solid State Physics* (Saunders, Orlando, FL, 1976).
[25]P. C. Pattnaik, M. D. Thompson, and T. P. Das, Phys. Rev. B **16**, 5390 (1977); **19**, 4326 (1979).
[26]F. D. Feilock and W. R. Johnson, Phys. Rev. **187**, 391 (1969).
[27]J. Singh, S. K. Rattan, and S. Prakash, Phys. Rev. B **38**, 10 440 (1988).
[28]References cited in Ref. 2.